Improvement in the light outcoupling efficiency of organic light-emitting diodes using a hemispherical lens and a multipatterned one-dimensional photonic crystal fabricated by autocloning



2015 Appl. Phys. Express 8 082102

(http://iopscience.iop.org/1882-0786/8/8/082102)

Applied Physics Express **8**, 082102 (2015)
http://dx.doi.org/**10.7567/APEX.8.082102**

# Improvement in the light outcoupling efficiency of organic light-emitting diodes using a hemispherical lens and a multipatterned one-dimensional photonic crystal fabricated by autocloning

Hiroshi Fujimoto[1,2], Masayuki Yahiro[1,2,3], Takayuki Kawashima[4], Keisuke Konno[5], Qiang Chen[5], Kunio Sawaya[6], Shojiro Kawakami[4,6], and Chihaya Adachi[1,2,3,7,8*]

[1]*Fukuoka i$^3$-Center for Organic Photonics and Electronics Research (i$^3$-OPERA), Fukuoka 819-0388, Japan*
[2]*Center for Organic Photonics and Electronics Research (OPERA), Kyushu University, Fukuoka 819-0395, Japan*
[3]*Institute of System, Information Technology and Nanotechnology (ISIT), Fukuoka 819-0388, Japan*
[4]*Photonic Lattice, Inc., Sendai 989-3204, Japan*
[5]*Department of Communications Engineering, Tohoku University, Sendai 980-8579, Japan*
[6]*Sendai Foundation for Applied Information Sciences, Sendai 980-0012, Japan*
[7]*Japan Science and Technology Agency (JST), ERATO, Adachi Molecular Exciton Engineering Project, Fukuoka 819-0395, Japan*
[8]*International Institute for Carbon Neutral Energy Research (WPI-I$^2$CNER), Kyushu University, Fukuoka 819-0395, Japan*
E-mail: adachi@cstf.kyushu-u.ac.jp

Received June 5, 2015; accepted July 2, 2015; published online July 22, 2015

The outcoupling efficiency of organic light-emitting diodes was improved using a photonic crystal fabricated by autocloning, which has potential advantages for mass production. By using layer thicknesses optimized by optical simulations, the experimental external quantum efficiency of a device with the photonic crystal and a hemispherical lens was 43.4%, which is 2.13 times that of a device on a flat substrate without the lens. Comparisons with the simulated distributions of the light modes in the devices show that the photonic crystal reduces the light loss from the waveguide and evanescent modes. The emission pattern was independent of substrate rotation. 

In recent years, significant advances have been made in organic light-emitting diodes (OLEDs), resulting in their application in smartphones and large-screen televisions.[1)] Flexible and large-area lighting devices that take advantage of the unique properties of OLEDs compared with inorganic devices are also under development to realize new functionalities.[2,3)] However, the external quantum efficiency ($\eta_{ext}$) of conventional OLEDs fabricated on conventional, flat substrates is limited to 20–25% even when the internal quantum efficiency ($\eta_{int}$) is close to 100% because of various optical losses.[4–8)]

One major source of optical losses is the use of organic layers and a transparent electrode, usually indium–tin oxide (ITO), with typical refractive indexes of 1.7–2.0 and a glass substrate with a refractive index of 1.51. Such high refractive indexes relative to that of air result in the total internal reflection and trapping of light in the glass and device layers, called the substrate and waveguide modes, respectively. Another significant source of losses is the generation of evanescent waves such as surface plasmons at the interface between the cathode and organic layers caused by the short distance (several tens of nanometers) between the light-emitting recombination zone and the cathodes. For conventional OLEDs, nearly half of the generated light is estimated to be lost to evanescent modes, while approximately 15% is lost to waveguide modes and 20% to substrate modes.[6–8)] Therefore, improving the efficiency of light outcoupling from OLEDs is critical for increasing $\eta_{ext}$ and has been the subject of significant research and development.

Two common techniques for extracting substrate modes are the use of scattering layers and the application of a microlens array to the outer substrate surface.[9–11)] The contributions of waveguide and evanescent modes have been reduced by fabricating device active layers on top of substrates structurally patterned with pillar arrays and corrugated surfaces, which can be periodic to form photonic crystals or random.[12–16)] The structured surface suppresses the formation of waveguide modes and the propagation of surface plasmons, leading to an increase in outcoupling efficiency. Nanoimprinting, which can be adopted for mass production, has been used to fabricate photonic crystals by hot embossing ultraviolet-curable polymer resins or glass having low glass-transition temperatures ($T_g$).[14–16)] However, the angular surfaces of the imprinted patterns can cause serious problems such as high leakage current. To smooth the surface, $SiN_x$ deposited by plasma-enhanced chemical vapor deposition has been used as a planarization layer,[15,16)] but the deposition of the $SiN_x$ layer on the pattern disturbs the emission spectra because of its mismatched refractive index and increases the deposition cost. Furthermore, $SiN_x$ has stronger absorption in the visible spectrum than the glass generally used as the substrate.

In this study, we used an autocloning method that is suitable for mass production to build a smooth face of $SiO_2$ on a multipatterned one-dimensional photonic crystal etched into the substrate surface for improved light extraction.[17)] This method duplicates the surface shape of the structured substrate to successive layers deposited via the sputtering of $SiO_2$ by including an etching step using ions incident to the substrate after each layer deposition. This process can be controlled by adjusting the rates of deposition and etching. Here, we use the autocloning method to transform the surface of the photonic crystal from jagged and sharp to smooth and wavy, making it suitable for OLEDs, which are generally sensitive to sharp protrusions on the substrate. The use of conventional sputtering equipment, which is well established for the mass production of LCDs[18)] and has also been demonstrated for the fabrication of OLED cathodes,[19)] reduces the barrier for applying this process to mass production.

The initial photonic crystal is etched directly into the glass substrate surface instead of being formed in a resin layer deposited on the substrate surface, eliminating the resin from the final device, which can be a source of impurities. Forming the initial pattern by etching also allows for a wide range of glasses to be used instead of the expensive low-$T_g$ glass that

 

is necessary when the pattern is directly nanoimprinted into the glass. By using sputtered $SiO_2$ to smooth the photonic structure without planarizing it, we can overcome the problems related to the cost, absorption, and mismatched refractive index of $SiN_x$ planarization. Although we use electron beam (EB) lithography to pattern a resist before etching the substrate in this experiment, nanoimprinting of the resist can be used in the future to scale up the process. Additionally, the autocloning method exhibits a self-healing effect that results in a highly reliable structure even when defects occur in the base structure, which will be especially advantageous for patterns formed by nanoimprinting.[20)]

In this paper, we report and evaluate the improvement in outcoupling efficiency using a multipatterned one-dimensional photonic crystal fabricated by autocloning. An OLED structure having layer thicknesses that maximize the outcoupling efficiency, which was optimized by optical simulations and confirmed experimentally, was used to reduce the possible overestimation of enhancement. As an emitter, a material exhibiting thermally delayed fluorescence (TADF), which can be used to obtain $\eta_{int}$ of nearly 100% without the need for a rare metal,[21,22)] was chosen. Measurements of device characteristics with a hemispherical lens on the face of the device to extract the substrate modes[23,24)] confirm the reduction of evanescent and waveguide modes by the photonic crystal. Finally, the optical simulation and experimental results are used to show that the $\eta_{int}$ of the TADF-based OLED should be approaching 100%.

A photonic crystal with a periodic pattern consisting of rectangular grooves covering an area of $5 \times 5\,mm^2$ in the center of a $25 \times 25\,mm^2$ quartz substrate was formed by patterning a resist layer on the quartz by EB lithography followed by the etching of the quartz and the removal of the resist. Smooth corrugated patterns, which serve as the base for the device, were fabricated by autocloning with deposition and etching cycles of $SiO_2$, which has the same refractive index ($n \sim 1.48$) as the substrate, on top of the structured quartz. Thin films (100 nm) of ITO ($n \sim 2.0$) were deposited on the substrates by sputtering in a compact sputtering system (ULVAC CS-L) and patterned by wet etching. Polyimide bank structures were spin-coated and patterned on the ITO to define an active device area of $0.01\,cm^2$ in the center of the substrate.

Next, the organic active layers of the OLEDs were deposited by thermal evaporation at a base pressure of $10^{-6}$ Pa on the substrates. The evaporated organic materials were 1,4,5,8,9,11-hexaazatriphenylenehexacarbonitrile (HAT-CN) as a hole injection layer, 9,9′,9″-triphenyl-9*H*,9′*H*,9″*H*-3,3′:6′,3″-tercarbazole (Tris-PCz) as a hole transport layer, 3,3-di(9*H*-carbazol-9-yl)biphenyl (mCBP) doped with (4s,6s)-2,4,5,6-tetra(9*H*-carbazol-9-yl)isophthalonitrile (4CzIPN) as an emitting layer, 2,4,6-tris(biphenyl-3-yl)-1,3,5-triazine (T2T) as a hole-blocking layer, and 2,7-bis(2,2′-bipyridine-5-yl)triphenylene (Bpy-TP2) as an electron transport layer (ETL). Finally, an electron injection layer and cathodes of LiF and Al were deposited by evaporation.

To evaluate the device characteristics, the current density ($J$)–voltage ($V$)–$\eta_{ext}$ characteristics and the angular dependence of the luminance were measured using an external quantum efficiency measurement system with the face of the device coupled to a 3.3-in. integrating sphere (Hamamatsu Photonics C9920-12), which prevents the measurement of edge emission, and a brightness light distribution characteristic measurement system (Hamamatsu Photonics C9920-11), respectively. The optical calculation software Setfos (Fluxim AG) was used for the optical simulations of the OLEDs. For the outcoupling of the substrate modes, a BK-7 hemispherical lens with a diameter of 10 mm was placed in close contact with the face of the device using a matching oil with a refractive index $n$ of 1.515 between the device and the lens.

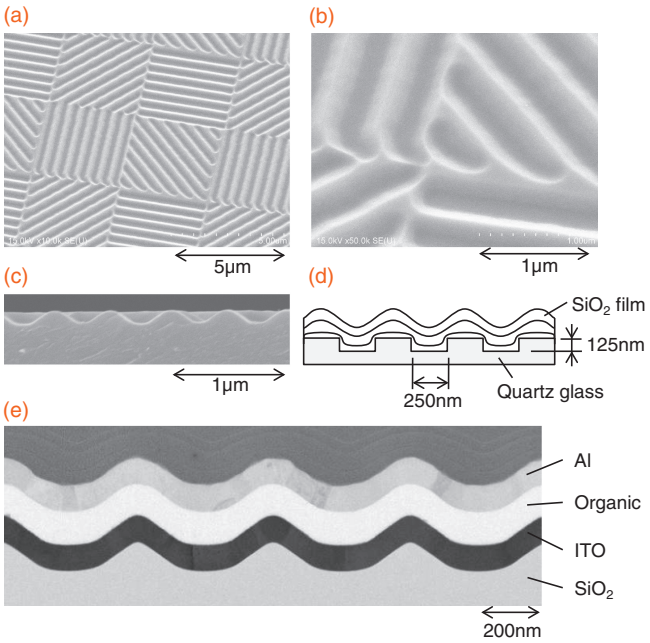


**Fig. 1.** (a)–(c) Scanning electron microscopy tomographic images of the photonic crystal substrate. (d) Schematic of the cross section of the photonic crystal substrate. (e) Bright-field scanning transmission electron microscopy tomographic image of the OLED on the photonic crystal substrate.

Figures 1(a)–1(d) show scanning electron microscopy tomographic views and a cross-sectional schematic of the photonic crystal consisting of a patterned quartz substrate covered with $SiO_2$ deposited by autocloning. The depth and pitch of the fabricated patterns are 125 and 500 nm, respectively [Fig. 1(d)]. The pitch was chosen to be close to the wavelength of emitted light for efficient diffraction while minimizing absorption, and the depth was chosen to limit the possibility of discontinuities originating from a high aspect ratio occurring in the ITO and organic layers. To obtain the same characteristics from devices deposited on the corrugated pattern regardless of how the device is rotated in the plane of the substrate, the periodic pattern consisted of four segments each with an area of $4 \times 4\,\mu m^2$ and ridges at angles of 0, 45, 90, or 135°. As seen in the expanded view, the boundaries between segments were well-defined and formed without defects.

On top of the substrates, ITO was deposited by sputtering and patterned by wet etching, polyimide bank structures were fabricated, and OLED layers were evaporated. The performance difference between the devices fabricated on flat quartz and on the photonic crystal was determined using green OLEDs (emission peak of 515 nm) having the structure ITO (100 nm)/HAT-CN (10 nm)/Tris-PCz (20 nm)/9% 4CzIPN:mCBP (30 nm)/T2T (10 nm)/Bpy-TP2 (50 nm)/LiF (0.8 nm)/Al (100 nm). The effect of layer thickness on

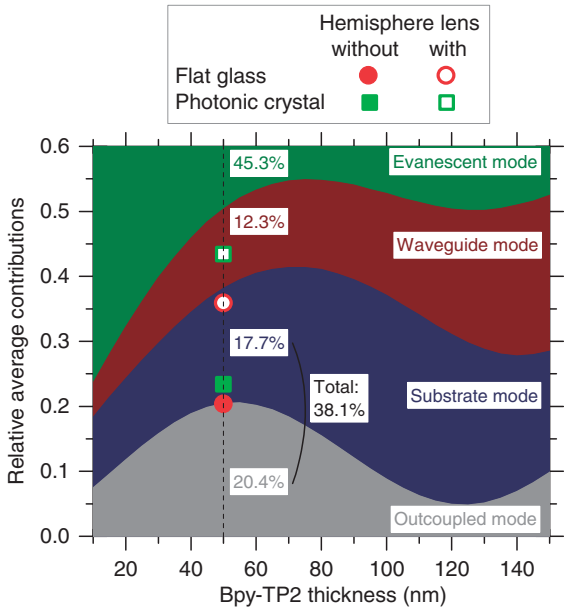


**Fig. 2.** Distributions of the light modes as a function of the ETL thickness calculated by optical simulation for a device on a flat substrate with the experimental results for $\eta_{ext}$ at $J = 1\,mA/cm^2$ also indicated.

outcoupling was simulated using optical calculation software. On the basis of the optical simulation results in Fig. 2, an ETL thickness of 50 nm was chosen to maximize the outcoupling efficiency in the conventional device on a flat substrate.

The bright-field scanning transmission electron microscopy tomographic image of the OLED on the photonic crystal substrate in Fig. 1(e) shows a cross-sectional view of the photonic crystal surface smoothed by the $SiO_2$ layers and the resulting structure of the OLED layers deposited on the surface. The OLED layers conformally follow the corrugated pattern of $SiO_2$ and maintain the smooth shape of the photonic crystal. Since such a smooth film can be formed, the OLED can be fabricated without defects even though the substrate surface is corrugated.

Figure 3 shows the $J$–$V$–$\eta_{ext}$ characteristics of OLEDs fabricated on flat quartz and on the photonic crystal both with and without the hemispherical lens. Without the lens, the $\eta_{ext}$ and power efficiency ($\eta_p$) at $J = 1\,mA/cm^2$ were 20.4% and 39.6 lm/W for the device on flat quartz, and 23.4% and 48.1 lm/W for the device on the photonic crystal, indicating 15 and 21% enhancements of $\eta_{ext}$ and $\eta_p$, respectively. For the devices with the hemispherical lens to extract the substrate modes, the improvement was even larger, with $\eta_{ext}$ and $\eta_p$ increasing from 35.9% and 67.9 lm/W on flat quartz to 43.4% and 89.3 lm/W on the photonic crystal, respectively. Thus, by using both the photonic crystal and hemispherical lens to improve outcoupling, $\eta_{ext}$ and $\eta_p$ that are 2.13 and 2.25 times, respectively, those for a conventional device on a flat substrate without a lens were achieved. Furthermore, the driving voltage was lower for the photonic crystal devices, which may be due to the increase in surface area caused by the corrugated pattern of the substrate and leads to the slightly larger improvement in $\eta_p$ than in $\eta_{ext}$. On the other hand, as shown in Fig. 3(b), the emission spectra of light emitted from the faces of the devices measured with an integrating sphere were not changed when the corrugated pattern was used.

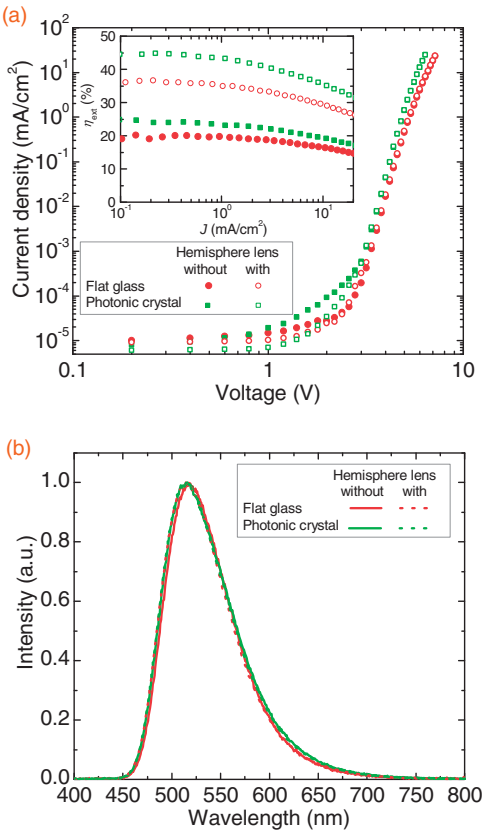


**Fig. 3.** (a) Experimental $J$–$V$ and (inset) $\eta_{ext}$–$J$ characteristics, and (b) emission spectra at $J = 1\,mA/cm^2$ for devices with the structure ITO (100 nm)/HAT-CN (10 nm)/Tris-PCz (20 nm)/9% 4CzIPN:mCBP (30 nm)/T2T (10 nm)/Bpy-TP2 (50 nm)/LiF (0.8 nm)/Al (100 nm) on flat quartz (reference) and on the photonic crystal both with and without the hemispherical lens.

Comparison of the experimental results at $J = 1\,mA/cm^2$ with the simulation results for an ETL of 50 nm in Fig. 2 shows that the $\eta_{ext}$ of 20.4% for the device on flat quartz is in good agreement with the outcoupling efficiency calculated by the optical simulations, indicating that the $\eta_{int}$ of the TADF device is close to 100%. Although 12.3 and 45.3% of the light are expected to be lost through the waveguide and evanescent modes, respectively, the hemispherical lens should be able to extract much of the 17.7% of the light trapped in the substrate modes. The fact that the $\eta_{ext}$ of the flat quartz device with the hemispherical lens (35.9%) is similar to the total of the simulated outcoupled and substrate modes (38.1%) indicates that the lens extracts almost all of the light in the substrate modes and further supports that the $\eta_{int}$ is approaching 100%. The residual 2.2% of $\eta_{ext}$ not extracted by the hemispherical lens can be attributed to the light emitted at angles nearly parallel to the 0.5-mm-thick substrate not coupling into the lens and exiting the edges of the substrate.

By including the photonic crystal, the waveguide and evanescent modes were expected to be decreased relative to the device on flat quartz. Comparison of the $\eta_{ext}$ of the device with the photonic crystal and hemispherical lens (43.4%) and the total of the simulated outcoupled and substrate modes for the flat quartz device (38.1%) shows that $\eta_{ext}$ surpasses the maximum expected without the photonic crystal. These results further confirm that the photonic crystal increases the outcoupling efficiency by reducing the amount of light confined in the waveguide and evanescent modes.

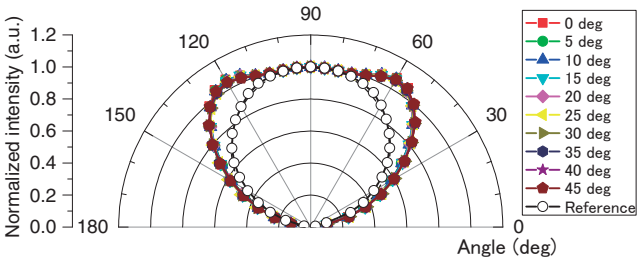


**Fig. 4.** Angular dependence of the luminance for the device on the photonic crystal when the substrate is rotated in plane from 0 to 45° and for the device on flat quartz (reference), both without the hemispherical lens.

Finally, the effect of the photonic crystal on the emission pattern was evaluated. Figure 4 shows the angular dependence of the luminance for devices on the flat quartz and photonic crystal, both without the hemispherical lens. Compared with the Lambertian emission pattern for flat quartz, the luminance with the photonic crystal increased in the range of 30 to 70°. Furthermore, the angular dependence of the luminance when the device with the photonic crystal was rotated from 0 to 45° in the plane of the substrate was found to be nearly identical at every angle, which is a result of using a periodic structure with four segments of rotating corrugated patterns (Fig. 1).

By using the photonic crystal, outcoupling efficiency could be improved, and $\eta_{ext}$ of 43.4% was obtained when used in conjunction with a hemispherical lens. This improvement over both the experimental and calculated values for a device on flat quartz indicates that the amount of light confined in the waveguide and evanescent modes is reduced by using the photonic crystal. The emission pattern was nearly independent of the in-plane substrate rotation because of the segmented periodic structure of the photonic crystal. The good agreement between the experimental $\eta_{ext}$ and outcoupling efficiency calculated by optical simulations for devices on flat quartz indicate that the $\eta_{int}$ of the TADF-based OLED is close to 100%. In future practical applications, the hemispherical lens can be replaced by a film containing a scattering layer or an array of microlenses to extract the light in the substrate modes of the device. The scattering effect of such films would also help to make the emission pattern with the photonic crystal more Lambertian. The results of this study are expected to advance the development of light-extracting substrates that can be fabricated for mass production.

**Acknowledgments** This work was supported in part by the Adaptable and Seamless Technology Transfer Program through target-driven R&D (A-STEP) and the International Institute for Carbon Neutral Energy Research (WPI-I$^2$CNER) sponsored by the Ministry of Education, Culture, Sports, Science and Technology (MEXT). H.F. also thanks Mr. Satoshi Yukiwaki, Ms. Kaori Nagayoshi, and Ms. Akiko Hamada from i$^3$-OPERA for their support of this study. The help of Dr. William J. Potscavage, Jr., of Kyushu University in the preparation of this manuscript is gratefully acknowledged. We also acknowledge Mr. Michinori Kitamura, Mr. Katsuya Imanishi, Mr. Makoto Maie, and Ms. Mayuko Kaji (Sumika Chemical Analysis Service, Ltd.) for the STEM tomographic view analyses.

1) Y. H. Tak, C. W. Han, H. S. Kim, B. C. Kim, J. W. Kim, T. S. Kim, B. S. Kim, C. H. Oh, S. Y. Cha, and B. C. Ahn, Proc. SPIE **8829**, 88290R (2013).
2) N. Ohsawa, S. Idojiri, K. Kumakura, S. Obana, Y. Kobayashi, M. Kataniwa, T. Ohide, M. Ohno, H. Adachi, N. Sakamoto, S. Yatsuzuka, T. Aoyama, and S. Yamazaki, SID Symp. Dig. Tech. Pap. **44**, 923 (2013).
3) T. Tsujimura, J. Fukawa, K. Endoh, Y. Suzuki, K. Hirabayashi, and T. Mori, J. Soc. Inf. Disp. **22**, 412 (2014).
4) C. Adachi, M. A. Baldo, M. E. Thompson, and S. R. Forrest, J. Appl. Phys. **90**, 5048 (2001).
5) N. C. Greenham, R. H. Friend, and D. D. C. Bradley, Adv. Mater. **6**, 491 (1994).
6) L. H. Smith, J. A. E. Wasey, I. D. W. Samuel, and W. L. Barnes, Adv. Funct. Mater. **15**, 1839 (2005).
7) S. Nowy, B. C. Krummacher, J. Frischeisen, N. A. Reinke, and W. Brütting, J. Appl. Phys. **104**, 123109 (2008).
8) R. Meerheim, M. Furno, S. Hofmann, B. Lüssem, and K. Leo, Appl. Phys. Lett. **97**, 253305 (2010).
9) T. Yamasaki, K. Sumioka, and T. Tsutsui, Appl. Phys. Lett. **76**, 1243 (2000).
10) C. F. Madigan, M. H. Lu, and J. C. Sturm, Appl. Phys. Lett. **76**, 1650 (2000).
11) S. Möller and S. R. Forrest, J. Appl. Phys. **91**, 3324 (2002).
12) M. Fujita, T. Ueno, K. Ishihara, T. Asano, S. Noda, H. Ohata, T. Tsuji, H. Nakada, and N. Shimoji, Appl. Phys. Lett. **85**, 5769 (2004).
13) W. H. Koo, S. M. Jeong, F. Araoka, K. Ishikawa, S. Nishimura, T. Toyooka, and H. Takezoe, Nat. Photonics **4**, 222 (2010).
14) K. Ishihara, M. Fujita, I. Matsubara, T. Asano, S. Noda, H. Ohata, A. Hirasawa, H. Nakada, and N. Shimoji, Appl. Phys. Lett. **90**, 111114 (2007).
15) Y. R. Do, Y. C. Kim, Y. W. Song, and Y. H. Lee, J. Appl. Phys. **96**, 7629 (2004).
16) S. Jeon, J. W. Kang, H. D. Park, J. J. Kim, J. R. Youn, J. Shim, J. H. Jeong, D. G. Choi, K. D. Kim, A. O. Altun, S. H. Kim, and Y. H. Lee, Appl. Phys. Lett. **92**, 223307 (2008).
17) S. Kawakami, T. Kawashima, and T. Sato, Appl. Phys. Lett. **74**, 463 (1999).
18) Y. Sunaga, J. Vac. Soc. Jpn. **50**, 28 (2007) [in Japanese].
19) H. Fujimoto, T. Miyayama, N. Sanada, and C. Adachi, Org. Electron. **14**, 2994 (2013).
20) T. Kawashima, K. Miura, T. Sato, and S. Kawakami, Appl. Phys. Lett. **77**, 2613 (2000).
21) A. Endo, M. Ogasawara, A. Takahashi, D. Yokoyama, Y. Kato, and C. Adachi, Adv. Mater. **21**, 4802 (2009).
22) H. Uoyama, K. Goushi, K. Shizu, H. Nomura, and C. Adachi, Nature **492**, 234 (2012).
23) S. Reineke, F. Lindner, G. Schwartz, N. Seidler, K. Walzer, B. Lüssem, and K. Leo, Nature **459**, 234 (2009).
24) T. C. Rosenow, M. Furno, S. Reineke, S. Olthof, B. Lüssem, and K. Leo, J. Appl. Phys. **108**, 113113 (2010).